Published online 24 December 2012

Nucleic Acids Research, 2013, Vol. 41, No. 4 ***e56***
doi:10.1093/nar/gks1292

A novel non-radioactive primase–pyrophosphatase activity assay and its application to the discovery of inhibitors of *Mycobacterium tuberculosis* primase DnaG

Tapan Biswas[1], Esteban Resto-Roldán[1,2], Sean K. Sawyer[1], Irina Artsimovitch[3] and Oleg V. Tsodikov[1,*]

[1]Department of Medicinal Chemistry, College of Pharmacy, University of Michigan, 428 Church Street, Ann Arbor, MI 48109, USA, [2]Research Experiences for Undergraduates Program, College of Pharmacy, University of Michigan, 428 Church Street, Ann Arbor MI 48109, USA and [3]Department of Microbiology, Ohio State University, 105 Biological Sciences Building, 484 West 12th Avenue, Columbus, OH 43210, USA

Received August 31, 2012; Revised November 10, 2012; Accepted November 12, 2012

ABSTRACT

Bacterial DNA primase DnaG synthesizes RNA primers required for chromosomal DNA replication. Biochemical assays measuring primase activity have been limited to monitoring formation of radioactively labelled primers because of the intrinsically low catalytic efficiency of DnaG. Furthermore, DnaG is prone to aggregation and proteolytic degradation. These factors have impeded discovery of DnaG inhibitors by high-throughput screening (HTS). In this study, we expressed and purified the previously uncharacterized primase DnaG from *Mycobacterium tuberculosis* (*Mtb* DnaG). By coupling the activity of *Mtb* DnaG to that of another essential enzyme, inorganic pyrophosphatase from *M. tuberculosis* (*Mtb* PPiase), we developed the first non-radioactive primase–pyrophosphatase assay. An extensive optimization of the assay enabled its efficient use in HTS ($Z' = 0.7$ in the 384-well format). HTS of 2560 small molecules to search for inhibitory compounds yielded several hits, including suramin, doxorubicin and ellagic acid. We demonstrate that these three compounds inhibit *Mtb* DnaG. Both suramin and doxorubicin are potent (low-μM) DNA- and nucleotide triphosphate-competitive priming inhibitors that interact with more than one site on *Mtb* DnaG. This novel assay should be applicable to other primases and inefficient DNA/RNA polymerases, facilitating their characterization and inhibitor discovery.

INTRODUCTION

Primases, essential enzymes in all domains of life, synthesize primers for DNA replication (1). Bacterial primases (DnaG) are highly conserved, and they are distinct from their eukaryotic and archaeal counterparts (2–15). Therefore, DnaG is a novel and attractive antibacterial drug target. By using single-stranded DNA (ssDNA) as a template, DnaG synthesizes short (<30-nt) RNA primers that are then extended by the replicative DNA polymerase (Pol III) in the process of chromosomal DNA replication (16). Because DnaG is an inefficient and weakly processive RNA polymerase (17–22), traditional priming activity assays (23,24), including the only reported assay used in high-throughput screening (HTS) (25), use radioactively labelled nucleotide triphosphates for detection of the priming reaction products. Despite the weak activity of DnaG, such priming activity assays with primase alone have been reported (18,21,22). To boost the primase activity for its detection, other accessory DNA replication proteins, such as ssDNA binding protein or DnaB helicase, have been commonly used. The only previously reported non-radioactive primase activity assay potentially applicable to HTS is a fluorometric assay based on the increase of fluorescence of PicoGreen dye with RNA–DNA duplex formation (26). This assay is expected to work efficiently when the primers made in the assay are long (>6 nt), so that they form a stable duplex with DNA, needed for robust PicoGreen fluorescence enhancement. A shortcoming of fluorometric assays in their use in HTS is a possible interference of aromatic or non-polar compounds with the signal because of their interactions with the fluorescent label.

*To whom correspondence should be addressed. Tel: +1 734 936 2676; Fax: +1 734 647 8430; Email: olegt@umich.edu

HTS using radioactivity demands rigorous safety measures, generates large amounts of liquid waste and is costly. For these reasons, use of radioactivity in most academic HTS facilities is not feasible. A non-radioactive and quantitative primase assay, as the one we have developed in this study, is highly desirable for HTS as well as for a more facile characterization of primases and other inefficient nucleic acid polymerases.

To develop the primase assay, we chose the previously uncharacterized DnaG from *Mycobacterium tuberculosis* (*Mtb* DnaG), the deadliest bacterial pathogen. A highly optimized purification procedure for *Mtb* DnaG and identification of conditions that maximize its steady-state nucleotidyl transferase activity reported here enabled us to develop a novel robust primase activity assay. In this assay, we use another essential bacterial protein, inorganic pyrophosphatase (PPiase) (27) as a coupled enzyme. PPiase selectively cleaves pyrophosphate (PP_i) into two phosphates (P_i) and does not hydrolyse nucleotide triphosphates, thus allowing us to monitor PP_i release through detection of P_i (28,29). *In vivo*, the cleavage of PP_i by PPiase is used to drive otherwise reversible nucleotide transfer reactions, in which a nucleotide monophosphate is transferred from a nucleotide triphosphate (NTP) onto a substrate with the release of PP_i. These types of reactions include chromosomal DNA synthesis as well as the fatty acid adenylation, a critical biochemical step in fatty acid metabolism. In fact, inorganic pyrophosphatases from yeast and *Escherichia coli* were previously used in coupled assays with other enzymes, such as protein prenyltransferases (30), adenylate cyclase (31), acetyl-CoA synthetase (32) and aminoacyl-tRNA synthetase (33). In our assay, we use PPiase from *Mtb* (162 amino acid residues), which shares a modest (30%) amino acid residue sequence identity to its human counterpart, PPA1 (289 residues). The considerable divergence between PPA1 and *Mtb* PPiase, including residue differences in the active sites of these two enzymes (34), implies a possibility of discovering an inhibitor selective for *Mtb* PPiase.

Conceptually novel anti-tuberculosis drugs are acutely needed in clinics because of the alarming spread of multidrug-resistant strains of *Mtb*. Herein, we report the development of a new coupled primase–pyrophosphatase assay that exploits two novel attractive bacterial targets, *Mtb* DnaG and *Mtb* PPiase, for inhibitor discovery.

MATERIALS AND METHODS

Cloning and purification of *Mtb* DnaG

The primase gene *dnaG* (locus tag: Rv2343c) was amplified by polymerase chain reaction from *Mtb* H37Rv genomic DNA (BEI Resources, NIAID, NR-14865) by using primers (5′-AGTTAGCACATATGTCCGGCCGGATC TCCG-3′) and (5′-CCGCTCGAGTCACGCGGTGAGA TCG-3′) and cloned between NdeI and XhoI sites of a modified pET19b vector (35), encoding an N-terminal decahistidine tag separated from the recombinant protein by a PreScission protease (GE Healthcare, Piscataway, NJ, USA) cleavage site. The construct expressing *Mtb* DnaG E268Q was generated by mutagenesis of the aforementioned construct with a QuikChange Kit (Qiagen, Valencia, CA, USA) by using primers 5′-CATCA GGCCGTCGTCGTCCAGGGCTACACCGATGTCA TG-3′ and 5′-CA TGACATCGGTGTAGCCCTGGACG ACGACGGCCTGATG-3′. The wild-type and the mutant proteins were expressed and purified analogously. Protein expression was carried out in BL21 (DE3) cells cultured in LB broth. The culture was induced with 0.5 mM of IPTG at an attenuance of 0.2 and then incubated for 16 h at 18°C. All purification steps were carried out at 4°C. The cell pellet from a 4 l culture was suspended in 100 ml of buffer A [40 mM Tris–HCl pH 8.0, 600 mM of NaCl, 10% of glycerol, 1 mM of PMSF, 0.5 mM of adenosine triphosphate (ATP), 2 mM of $MgCl_2$ and 2 mM of β-mercaptoethanol] containing two tablets of complete ethylenediaminetetraacetic acid (EDTA)-free protease inhibitor cocktail (Roche Applied Science, Indianapolis, IN, USA). The cells were disrupted by sonication on ice and clarified by centrifugation at 38 000*g* for 60 min. The supernatant was filtered through a 0.45 μm Millex-HV PVDF filter (Millipore, Billerica, MA, USA) and applied to a 5 ml Ni-IMAC HisTrap FF column (GE Healthcare) equilibrated with buffer A. The column was washed with 120 ml of buffer A containing 50 mM imidazole, and then protein was eluted with 11 ml of buffer A containing 500 mM imidazole. The eluate was adjusted to NaCl of 200 mM, with buffer A prepared without NaCl and digested overnight at 4°C with PreScission protease. The digested protein was purified on a size-exclusion S-200 column (GE Healthcare) equilibrated in buffer B (40 mM Tris–HCl pH 8.0, 600 mM of NaCl, 10% of glycerol, 0.25 mM of ATP, 2 mM of $MgCl_2$ and 2 mM of β-mercaptoethanol), and the protein-containing fractions were pooled and concentrated using an Amicon Ultra-15 centrifugal filter device (Millipore) to 5 mg/ml. The enzyme was stored on ice for all assays. The recombinant untagged DnaG was highly homogeneous (Coomassie blue staining indicated >95% purity) and remained stable and active, while on ice, for 2 weeks. One hour before the assays, the storage buffer was exchanged by MicroSpin G-25 columns (GE Healthcare) into buffer C (40 mM of HEPES–NaOH pH 7.5, 600 mM of NaCl, 10% of glycerol, 2 mM of $MgCl_2$, 2 mM of β-mercaptoethanol and 0.1 of mM ATP). The presence of ATP in the protein buffer results in 10 μM ATP in the reaction mixture. This low concentration of ATP is negligible, as it is below K_m for ATPases and other ATP-interacting enzymes, including *Mtb* DnaG. Partial degradation of such a small amount of ATP, even if it occurred, would be below or at the detection limit of our assay.

Purification of *Mtb* PPiase

The pJ411 vector (DNA2.0, Menlo Park, CA, USA) encoding *Mtb* PPiase bearing an N-terminal hexahistidine-tag was a generous gift from Dr Luiz Pedro Carvalho. *Mtb* PPiase was expressed similarly to *Mtb* DnaG. All purification steps were carried out at 4°C. The cell pellet was resuspended in 20 mM of TEA buffer pH 7.8. The cells were disrupted sonication and clarified by centrifugation at 25 000*g* for 30 min.

The supernatant was applied to a 5 ml Ni-IMAC HisTrap FF column (GE Healthcare) equilibrated with buffer A (20 mM TEA pH 7.8, 50 mM of imidazole and 300 mM of NaCl). The column was washed with 220 ml of buffer A, and protein was eluted with a linear gradient of 50–500 mM of imidazole in buffer A (570 ml). The fractions containing *Mtb* PPiase were pooled, concentrated and passed through a size-exclusion S-200 column (GE Healthcare) equilibrated in 40 mM of Tris–HCl pH 8.0, 100 mM of NaCl. The fractions containing protein were pooled and concentrated using an Amicon Ultra-15 centrifugal filter device (Millipore) to 750 μM. The recombinant His-tagged *Mtb* PPiase was highly homogeneous (Coomassie blue staining indicated >98% purity) and stable at 4°C for 6 months.

Coupled colorimetric primase–pyrophosphatase assay (optimization of conditions)

In all coupled primase–pyrophosphatase assays that were carried out during the optimization phase to determine DNA template (sequence and length), divalent metal type and concentration, buffer type and pH and in time course experiments, we mixed DNA (Integrated DNA Technologies, Coralville, IA, USA), buffer, NTP (Promega, Madison, WI, USA) and pyrophosphatase on ice and then added *Mtb* DnaG, so that the reagent mixture is at twice the intended concentration of all reagents. The mixture was then diluted two-fold with water to give the final concentration of *Mtb* DnaG (0.7 μM or as specified) DNA (1.25 μM or as specified), NTP (110 μM or as specified), NaCl (50 mM), KGlu (150 mM), buffer (20 mM of CAPS pH 8.8 or as specified) and divalent metals (2 mM of Mn^{2+} and 1 mM of Mg^{2+} or as specified). *Mtb* DnaG alone is prone to severe aggregation and rapidly becomes inactive at salt concentrations <275 mM. However, in the presence of DNA and nucleotides, *Mtb* DnaG maintains its solubility and activity. The reaction mixture was incubated at room temperature (22°C) for 30 min. In the assay optimization experiments, inorganic pyrophosphatase from *Saccharomyces cerevisiae* (Sigma-Aldrich, St. Louis, MO, USA) was used in a three-fold excess of the minimal concentration needed for complete PP_i cleavage (as determined experimentally for each enzyme stock). The yeast enzyme was replaced by *Mtb* PPiase in the HTS and in the mode of inhibition studies. The P_i formed as a consequence of breakdown of the released PP_i was quantitated using procedures adapted from earlier studies (36). In brief, 150 μl of the malachite green reagent (MGR; a 2:1:1:2 mixture of 0.0812% malachite green, 2.32% w/v polyvinyl alcohol, 5.72% in 6 M of HCl ammonium molybdate and water) was added to 30 μl reactions and followed by addition of 15 μl of 34% sodium citrate after 1 min. After allowing colour to develop for 30 min, absorbance at 620 nm was measured with a Biotek Synergy H1 plate reader (Biotek, Winooski, VT, USA). In all coupled primase–pyrophosphatase assays, we calibrated the absorbance at 620 nm to the concentration of P_i (twice that of PP_i) by using sodium phosphate and verified the linearity of the signal in the experimental range (the signal was linear up to Abs = 1.5). For the assay optimization and inhibitor characterization, we used flat-bottom 96-well clear polystyrene plates (Fisher Scientific, Pittsburgh, PA, USA).

Primer synthesis assay

Primer synthesis reactions to observe the radiolabelled RNA products were carried out under conditions similar to those determined in the course of the optimization of conditions by the coupled primase–pyrophosphatase assay. More specifically, the reactions were carried out in buffer containing DNA (1 μM; the sequences are specified in the text), NTP (100 μM) in 20 mM of CAPS pH 8.8, 150 mM of KGlu containing divalents (Mn^{2+} or Mg^{2+}), DTT (1 mM) and 110 nM of α–^{32}P-GTP. The products were extracted with phenol and run in a 12% urea–polyacrylamide gel. The gels were exposed to phosphorimager plates and read in a Typhoon phosphorimager system (GE Healthcare).

High-throughput screening assay

For its performance in HTS, we adapted the assay so that it can sustain the manipulations at room temperature for 4–6 h without any significant deleterious effects on the protein or other reagents. Fifty nanomolars of *Mtb* PPiase, instead of yeast PPiase, was used in the HTS and inhibitor characterization. To minimize the number of injections and error in dispensing reagents using liquid handling robotics, we revised the assay protocols. Small molecule compounds were dispensed into 384-well flat bottom, non-binding surface, polystyrene plates (Corning Incorporated, Corning, NY, USA) from the compound library plates with a Biomek FX robot (Beckman Coulter, Brea, CA, USA) with 200 nl of inhibitors (to obtain the final concentration in the reaction of 13 μM). Twenty microlitres of the NTP mix (with 2 mM of β-mercaptoethanol) in water was then added to all wells. EDTA at the final concentration of 30 mM was added to the last two columns of wells as a positive inhibition control. Finally, a 10 μl mixture of DNA, *Mtb* PPiase and *Mtb* DnaG in the appropriate buffer (at three-fold higher concentrations of all reaction and buffer components than their final concentrations) was added. After 30 min incubation at room temperature, 30 μl of the MGR was added followed by 10 μl of 10% sodium citrate, and plates were shaken briefly. Absorbance at 620 nm was read in 30 min with a PHERAstar plate reader (BMG Labtech, Cary, NC, USA). This assay was used to screen a library of 2556 small molecules comprising 2000 food and drug administration-approved drugs (Spectrum Chemicals, New Brunswick, NJ, USA), 450 molecules that have been used in human therapy (NIH Clinical Collection) and 106 kinase inhibitors (Enzo Life Sciences, Farmingdale, NY, USA).

The Z' score was calculated for the pilot 384-well assay where DMSO was delivered without the small molecules, by using the following equation (37):

$$Z' = 1 - 3\frac{\mathrm{SD(pos)} + \mathrm{SD(neg)}}{|\mathrm{Av(pos)} - \mathrm{Av(neg)}|}$$

where Av(pos) and SD(pos) are the signal (absorbance) and its standard deviation for the positive controls (EDTA-containing reactions), and Av(neg) and SD(neg) are the respective values for negative controls (DMSO-containing reactions).

Dose–response assays

For the mode of inhibition studies, the reactions were carried out under conditions similar to those used in the HTS, except the volumes of the colour reagents were slightly modified to adapt it to the 96-well plate and to further increase the stability and consistency of the colour formation. In these assays, 90 µl of MGR was added to a 30 µl reaction mixture followed by 30 µl of 10% sodium citrate.

Reactions were carried out with [*Mtb* DnaG] = 0.5 µM, [DNA] = 1.25 µM, [NTP] = 110 µM at different concentrations of inhibitors, as specified in the text. Relative activities were calculated by dividing the concentrations of PP_i released in the priming reactions in the presence of inhibitors by that released in its absence. The following dose–response equation was used to fit these data with SigmaPlot 9.0 (SysStat Software, San Jose, CA, USA), with IC_{50} and the Hill coefficient n as the fitting parameters:

$$f = \frac{1}{1 + \left(\frac{[\mathrm{I}]}{IC_{50}}\right)^n}$$

Analysis of mode of inhibition assays

The assays were performed with *Mtb* DnaG (0.5 µM) and *Mtb* PPiase (50 nM) in the same reaction buffer as that used in the HTS assays. The steady-state rate of PP_i release was calculated based on measurements of the concentration of released PP_i in 20-min reactions, as described earlier in the text. Two sets of reactions were run: (i) at constant [DNA] = 1.25 µM at different concentrations of NTP (31.25, 62.5, 125, 250 and 500 µM) and (ii) at constant [NTP] = 110 µM at different concentrations of DNA (0.19, 0.38, 0.75 and 1.5 µM). We observed inhibition of P_i generation by NTP and DNA at higher NTP and DNA concentrations beyond the aforementioned ranges; therefore, they were not used in this analysis. For each pair of DNA and NTP concentrations, different concentrations of the inhibitors (suramin and doxorubicin) were used (0, 1.25, 2.5, 5, 10, 20 and 40 µM). As a simplifying approximation, to analyse the data, we used an ordered sequential rapid equilibrium mechanism of RNA synthesis by DnaG, in which DNA binds free DnaG first, followed by binding of the first NTP and subsequent binding and incorporation of an average of m nucleotides (releasing m PPi molecules) and dissociation of DnaG from DNA:

$$\mathrm{DnaG} + \mathrm{DNA} \overset{K_{\mathrm{DNA}}}{\rightleftarrows} \mathrm{DnaG}\bullet\mathrm{DNA} + \mathrm{NTP} \overset{K_{\mathrm{NTP}}}{\rightleftarrows} \mathrm{DnaG}\bullet\mathrm{DNA}\bullet\mathrm{NTP} \overset{k_{\mathrm{cat}}}{\rightarrow} \mathrm{DnaG} + \mathrm{DNA}\bullet\mathrm{primer} + m\mathrm{PP_i} + m\mathrm{NTP}$$

Here, K_{DNA} and K_{NTP} are equilibrium constants for binding primed DNA and NTP, respectively, both defined for the dissociation direction. This mechanism assumes that the concentration of NTP affects only initiation of primer synthesis. If the first NTP incorporation is slow (primer nucleation) relative to the m-1 subsequent incorporation steps (elongation), then k_{cat} is the catalytic rate constant of the slow nucleation step.

Because the data exhibit competitive inhibition with respect to both DNA and NTP and the inhibitor:target stoichiometry higher than 1:1 (model-independent observations), we considered the simplest competitive inhibition mechanism, in which an inhibitor (I) can bind non-cooperatively to n binding sites on *Mtb* DnaG:

$$\mathrm{DnaG} + \mathrm{I} \rightleftarrows \mathrm{DnaG}\bullet\mathrm{I}$$
$$\mathrm{DnaG}\bullet\mathrm{I} + \mathrm{I} \rightleftarrows \mathrm{DnaG}\bullet\mathrm{I}_2$$
$$\ldots$$
$$\mathrm{DnaG}\bullet\mathrm{I}_{n-1} + \mathrm{I} \rightleftarrows \mathrm{DnaG}\bullet\mathrm{I}_n$$

We designate as K_i an intrinsic equilibrium constant for binding of an inhibitor molecule to a site on DnaG, defined for the dissociation direction. This mechanism yields the following equation for the steady-state rate of PP_i release (V) in large excess of NTP and inhibitor, but not DNA, over *Mtb* DnaG:

$$V = \frac{k_{\mathrm{cat,app}}[\mathrm{DnaG}][\mathrm{DNA}][\mathrm{NTP}]}{K_{\mathrm{DNA}}K_{\mathrm{NTP}}} \quad (1)$$

Because one nucleation event leads to release of m PPi molecules, $k_{\mathrm{cat,app}} = mk_{\mathrm{cat}}$. The concentrations of free *Mtb* DnaG, [DnaG] and all DNA species not bound to DnaG, [DNA], are obtained from the conservation of material equations for DnaG and DNA and from the aforementioned equilibria as:

$$[\mathrm{DnaG}] = \frac{-b + \sqrt{b^2 - 4ac}}{2a}, \quad (2)$$

where

$$a = \left(\frac{K_{\mathrm{NTP}} + [\mathrm{NTP}]}{K_{\mathrm{NTP}}K_{\mathrm{DNA}}}\right)\left(1 + \frac{[\mathrm{I}]}{K_i}\right)^n, \quad (3)$$

$$b = \left(1 + \frac{[\mathrm{I}]}{K_i}\right)^n + \left(\frac{K_{\mathrm{NTP}} + [\mathrm{NTP}]}{K_{\mathrm{NTP}}K_{\mathrm{DNA}}}\right)\left([\mathrm{DNA}]_{\mathrm{T}} - [\mathrm{DnaG}]_{\mathrm{T}}\right), \quad (4)$$

$$c = -[\mathrm{DnaG}]_{\mathrm{T}}, \quad (5)$$

$$[\mathrm{DNA}] = [\mathrm{DnaG}]\left(1 + \frac{[\mathrm{I}]}{K_i}\right)^n + [\mathrm{DNA}]_{\mathrm{T}} - [\mathrm{DnaG}]_{\mathrm{T}} \quad (6)$$

Here, $[\mathrm{DnaG}]_{\mathrm{T}}$ and $[\mathrm{DNA}]_{\mathrm{T}}$ are the total concentrations of *Mtb* DnaG and DNA in the reaction, respectively. This rate law was globally fit to all the data collected for each inhibitor by using non-linear regression with SigmaPlot 9.0, with $k_{\mathrm{cat,app}}$, K_{DNA}, K_{NTP} and K_i as fitting parameters for different fixed integer values of n. A satisfactory fit was not obtained for $n = 1$ or $n = 2$ for either suramin or doxorubicin, consistent with the model-independent dose–response analysis. For suramin, the data were well fit for $n = 4$, whereas for doxorubicin, an equally good fit was produced for $n = 3$, yielding the best fit parameter

values and the theoretical curves generated by using these as presented in the 'Results' section. The data could be fit equally well by a more complex model, in which the inhibitors bind *Mtb* DnaG with high cooperativity, with $n = 3$ and $n = 2$ for suramin and doxorubicin, respectively. However, because the cooperative binding model contains too many fitting parameters to be resolved by the data, and because it lacks support by other experimental evidence, it is not presented here in further detail.

DNA-binding assay

DNA affinity of *Mtb* DnaG for ssDNA was measured at the conditions of the priming activity assays, either in the absence of NTPs or in the presence of all four NTPs, at [NTP] = 110 μM. We used a single-stranded 28-mer ssDNA: 5′-CCGAATCAGTCCGACGACGCATCAGC AC-3′, labelled at the 5′-end with 6-carboxyfluorescein (6FAM; Integrated DNA Technologies, Coralville, IA, USA). Titrations were set-up at the constant concentration of ssDNA of 20 nM at different concentrations of *Mtb* DnaG in separate 50 μl reaction mixtures and were equilibrated for 20 min at 22°C. Fluorescence anisotropy was monitored by a SpectraMax M5 plate reader (Molecular Devices, Sunnyvale, CA, USA), set at the excitation and emission wavelengths of 495 and 520 nm, respectively. To obtain equilibrium protein-DNA binding constant K_d, non-linear least-squares regression data fitting to the equilibrium 1:1 binding isotherm was performed with SigmaPlot 9.0 as previously described (38). No significant difference was observed between titrations in the presence or absence of NTPs; therefore, these data were averaged together.

RESULTS

Purification of *Mtb* DnaG

Expression and purification of *Mtb* DnaG have not been previously reported. Initially, we tested a variety of expression and purification protocols previously reported for other DnaG proteins; these efforts yielded inactive aggregated protein. During the extensive optimization of the purification procedure, we found that ATP (0.25 mM), NaCl (600 mM) and glycerol (~10%) all need to be present during all purification steps to prevent *Mtb* DnaG from aggregation. As a result, we obtained pure and active *Mtb* DnaG. The purified protein (Figure 1A) is homogeneous and monomeric as judged by S-200 size-exclusion chromatography (Figure 1B).

Development of a novel non-radioactive coupled primase–phosphatase assay

Primase activity has been historically monitored by visualization and quantification of radiolabelled RNA primers on a denaturing gel. We sought to develop a novel activity assay that would be robust (even at room temperature), would not require the use of radioactivity and would not require accessory factors, such as ssDNA-binding protein or DnaB helicase, which have been used previously to enhance primase activity. Such an assay would be highly suitable for high-throughput applications.

We developed a colorimetric coupled primase–pyrophosphatase assay satisfying these requirements (Figure 2). Inorganic pyrophosphatase (PPiase, type I) is used to cleave the pyrophosphate (PP_i) liberated in the priming reaction into phosphate (P_i). To measure the P_i concentration, we use the MGR (36), whose absorbance at 620 nm increases with increasing concentration of P_i, changing its colour from yellow to green. PPiase cleaves exclusively PP_i and does not exhibit any cleavage activity on NTP (29), a property that we also confirmed for yeast and *Mtb* PPiases. The concentration of PPiase was chosen to be three-fold higher than the minimum concentration required for cleavage of all released PP_i.

By monitoring synthesis of radiolabelled primers, we directly established that at the minimal conditions of our novel coupled assay, *Mtb* DnaG displays robust Mn^{2+}-dependent primer synthesis activity and has no detectable activity in Mg^{2+} (Figure 3). This activity is not highly processive, as evidenced by several short (<10 nt) products of different lengths, which is also observed with other primases (21). Because *Mtb* DnaG is an intrinsically inefficient polymerase, in developing the new assay, it was important to minimize any unwanted phosphate-borne signal from spurious ATPase activity that may be present in the protein preparations. Therefore, to avoid possible interference from ATPases, we designed a new

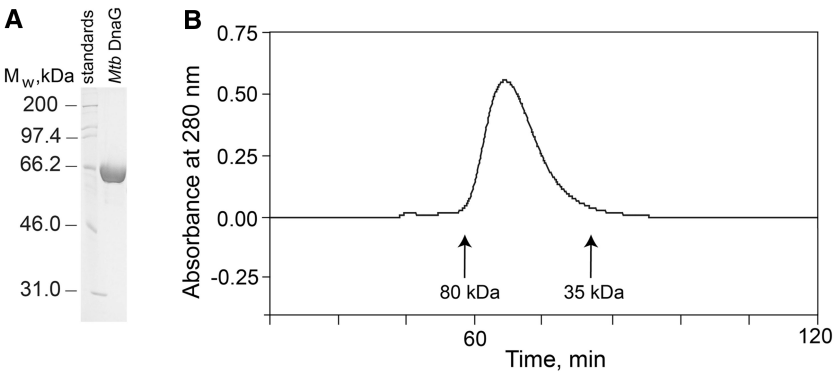

Figure 1. Purified *Mtb* DnaG. (**A**) A Coomassie-stained 12% sodium dodecyl sulphate–polyacrylamide gel electrophoresis of the purified *Mtb* DnaG showing its homogeneity. (**B**) The S-200 size-exclusion chromatogram of *Mtb* DnaG demonstrating its monomeric state.

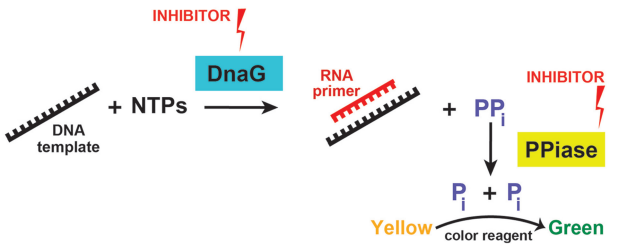

Figure 2. A schematic of the coupled colorimetric primase (DnaG)–pyrophosphatase (PPiase) assay.

DNA template (Figure 4, top inset). This template does not contain thymidine nucleotides in its 5′-half, so that ATP is not needed for the synthesis of complementary RNA; as a result, we could omit ATP in the reaction. Indeed, we obtained a robust DNA-dependent signal from the primer synthesis activity by *Mtb* DnaG in this reaction set-up with only CTP, GTP and UTP (Figure 4). An *Mtb* DnaG point mutant E268Q of a conserved divalent metal-coordinating residue (39) that is absolutely required for catalysis (21,40) was used as a control to ensure that the observed signal resulted specifically from the primer synthesis activity of *Mtb* DnaG. No signal was observed without the inorganic pyrophosphatase. We then performed the assay with a variety of divalent metal salts (Figure 5). The results confirmed the lack of detectable activity with Mg^{2+} and demonstrated that Mn^{2+} was the only divalent metal that supported robust activity among the seven metals tested. Mn^{2+} was previously reported to increase DnaG activity without significantly affecting other properties of DnaG (21). In a recently determined crystal structure of the catalytic core of *Staphylococcus aureus* DnaG in complex with nucleotides, a catalytic Mn^{2+} ion was shown to be interchangeable with Mg^{2+} (39).

Optimization of assay conditions

The colorimetric primase–pyrophosphatase assay provides a quantitative measure of kinetics of NTP incorporation into growing RNA by measuring PP_i release (Figure 6A). At these conditions ([*Mtb* DnaG] = 0.7 μM, [DNA] = 1.25 μM, [NTP (CTP, GTP, UTP)] = 110 μM each), the linear steady-state accumulation of PP_i persists until ~30 min from the start of the reaction, after which the signal starts to reach the plateau, likely because of accumulation of stable RNA–DNA duplexes or because of protein aggregation. Therefore, to obtain a robust signal in the steady-state measurements, a reaction time of 20–30 min (as specified) was chosen for further measurements. To find conditions that maximize the primer synthesis activity in our assay, we tested a variety of solution parameters. When measured as a function of the concentration of the divalent metal of choice, Mn^{2+}, *Mtb* DnaG exhibited a maximum activity near 2 mM of Mn^{2+} (Figure 6B). Mg^{2+} (1 mM) is used in the reaction to ensure robust activity of PPiase, which is not highly active in Mn^{2+} alone (34). Potassium glutamate (KGlu) was chosen for the assay, as it is the major electrolyte *in vivo* (41), and it significantly enhances protein–DNA

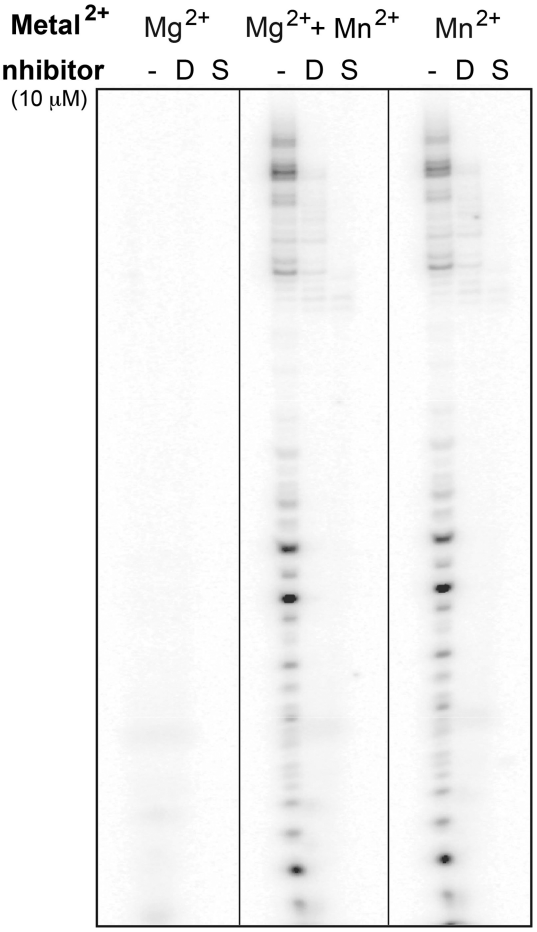

Figure 3. Synthesis of radiolabelled RNA primers by *Mtb* DnaG and its inhibition by 10 μM doxorubicin (D) and suramin (S). Phosphorimager analysis of a 12% of urea–polyacrylamide gel electrophoresis showing RNA products of the priming reaction. The priming reaction was performed with 1 mM of Mg^{2+}, 2 mM of Mn^{2+} and both on a 38-mer ssDNA template 5′-CTGGTGGGCCCAAACTTGATGC TCTAATACCGACGCGT-3′ in the presence of a mixture of the four nucleotides containing α-^{32}P-GTP.

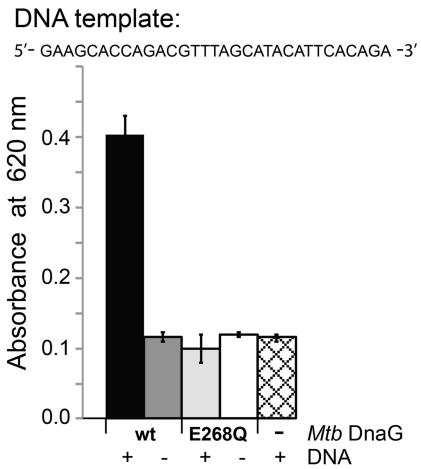

Figure 4. Representative coupled primase–pyrophosphatase reactions (a 30-min time point) with wild-type (wt) and E268Q mutant of *Mtb* DnaG.

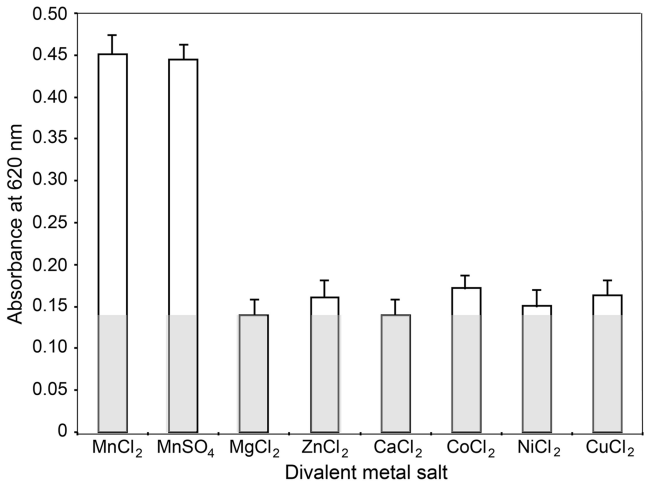

Figure 5. Activity of *Mtb* DnaG in the presence of different divalent metals, at 2 mM. The grey bars indicate the absorbance at time 0 in the reaction.

interactions *in vitro* (42). The activity was optimal in the physiological KGlu concentration range, 150–200 mM (Figure 6C). The primase was active in a variety of buffers and with pH values in the range 6.0–9.0 (Figure 6D); 20 mM of CAPS pH 8.8 was chosen, as it supported the highest activity of *Mtb* DnaG among the tested buffers and pHs.

The observed steady-state rate of PP_i release measured as a function of DNA concentration at [NTP] = 110 μM displayed a saturating behaviour indicative of tight binding of *Mtb* DnaG to DNA (a nearly linear increase of activity until half-saturation), with $K_{m,obs} < 0.3$ μM and $V_{max,obs} = 1.16 \pm 0.06$ μM/min (Figure 6E); the subscript 'obs' is used here to reflect the dependence of these parameters on the concentration of NTP. Only an upper bound on $K_{m,obs}$ (<0.3 μM) can be determined from this titration, because [*Mtb* DnaG] > K_m. Based on this dependence, we used [DNA] = 1.25 μM for HTS and inhibitor characterization, to maximize the signal and to ensure the sensitivity of the assay to potential inhibition. We observed a hyperbolic (Michaelis–Menten) saturation behaviour of the rate of PP_i release as a function of NTP concentration (at [DNA] = 1.25 μM; Figure 6F), yielding $K_{m,obs} = 177 \pm 7$ μM and $V_{max,obs} = 2.85 \pm 0.04$ μM/min. Note that the $V_{max,obs}$ value obtained in this assay is higher than that in the previous assay because [DNA] = 1.25 μM is saturating, whereas [NTP] = 110 μM is not. At [NTP] near 100 μM, a robust signal was achieved. Because less than a two-fold increase in signal required using five-fold higher concentrations of expensive high-purity NTPs in material-consuming HTS, we chose [NTP] = 110 μM for HTS.

High-throughput screening of 2560 compounds to discover inhibitors of *Mtb* DnaG and *Mtb* PPiase by the primase–pyrophosphatase assay

We adapted the assay to the 384-well format for its use in HTS of libraries of small molecules. To evaluate the suitability of the assay for HTS, we performed a control assay in a 384-well plate where DMSO solution (without small molecule compounds) was delivered into the reactions in all but 32 wells, and EDTA (at final concentration of 30 mM) was added in the remaining 32 wells as a positive inhibition control (Figure 7A). The inhibition by EDTA (manifested by the absence of the green colour of the MGR) was clearly distinguishable by the naked eye. The absorbance measurements in this control assay yielded a Z' score of 0.7, indicating that the assay is robust and suitable for HTS (37).

By using this assay, we carried out HTS of a library of 2556 diverse molecules, which comprised known drugs used in human therapy, natural products with undetermined biological activities, compounds in agricultural use and kinase inhibitors. The assay yielded nine different hits that displayed inhibition levels larger than three standard deviations (>3σ) of the negative controls on the same plate (Figure 7B). Three compounds (disopyramide phosphate, oleandomycin phosphate and fosfosal) displayed increase in absorbance. This was not because of enzyme activation, but because the first two compounds were phosphate salts and because phosphate was released on rapid hydrolysis of fosfosal at the acidic pH of the MGR (43). We performed dose–response measurements with three strong hits, suramin (7.2σ), doxorubicin (3.7σ) and ellagic acid (5.1σ) (Figure 8). These data yielded IC_{50} values of 6.3 ± 0.2 μM and 7.7 ± 0.5 μM for suramin and doxorubicin, respectively, indicating their potent inhibitory effects. Ellagic acid displayed approximately three-fold weaker inhibition ($IC_{50} = 22 \pm 3$ μM) and was not characterized further. None of the three compounds inhibited *Mtb* PPiase as assayed separately with inorganic pyrophosphate as a substrate, indicating that these compounds are bona fide *Mtb* DnaG inhibitors (the other six hits remain to be tested for DnaG and PPiase inhibition). The dose–response curves for suramin and doxorubicin could be well modelled only by using the Hill coefficients of 2.9 ± 0.1 and 2.0 ± 0.2, respectively (Figure 8), which indicates that the target contains multiple inhibitor-binding sites (44).

Mode of inhibition of *Mtb* DnaG by suramin and doxorubicin

We first confirmed directly that suramin and doxorubicin are potent *Mtb* DnaG inhibitors by observing their effect on the synthesis of radioactively labelled RNA products on the same DNA template at conditions similar to those of the colorimetric assay (Figure 9) and in assays with a different template DNA and with all four NTPs present in the reaction (Figure 3). To investigate the inhibitory mechanisms of suramin and doxorubicin in more detail, we measured the effect of these compounds on the steady-state accumulation of PP_i in the primer synthesis reaction. To determine whether suramin and doxorubicin interfere with interactions of *Mtb* DnaG with DNA, NTP or both, we performed measurements of the steady-state rate of PP_i release as a function of inhibitor concentration for different concentrations of DNA and NTP. One set of measurements was performed at a fixed concentration of DNA ([DNA] = 1.25 μM) with different concentrations of

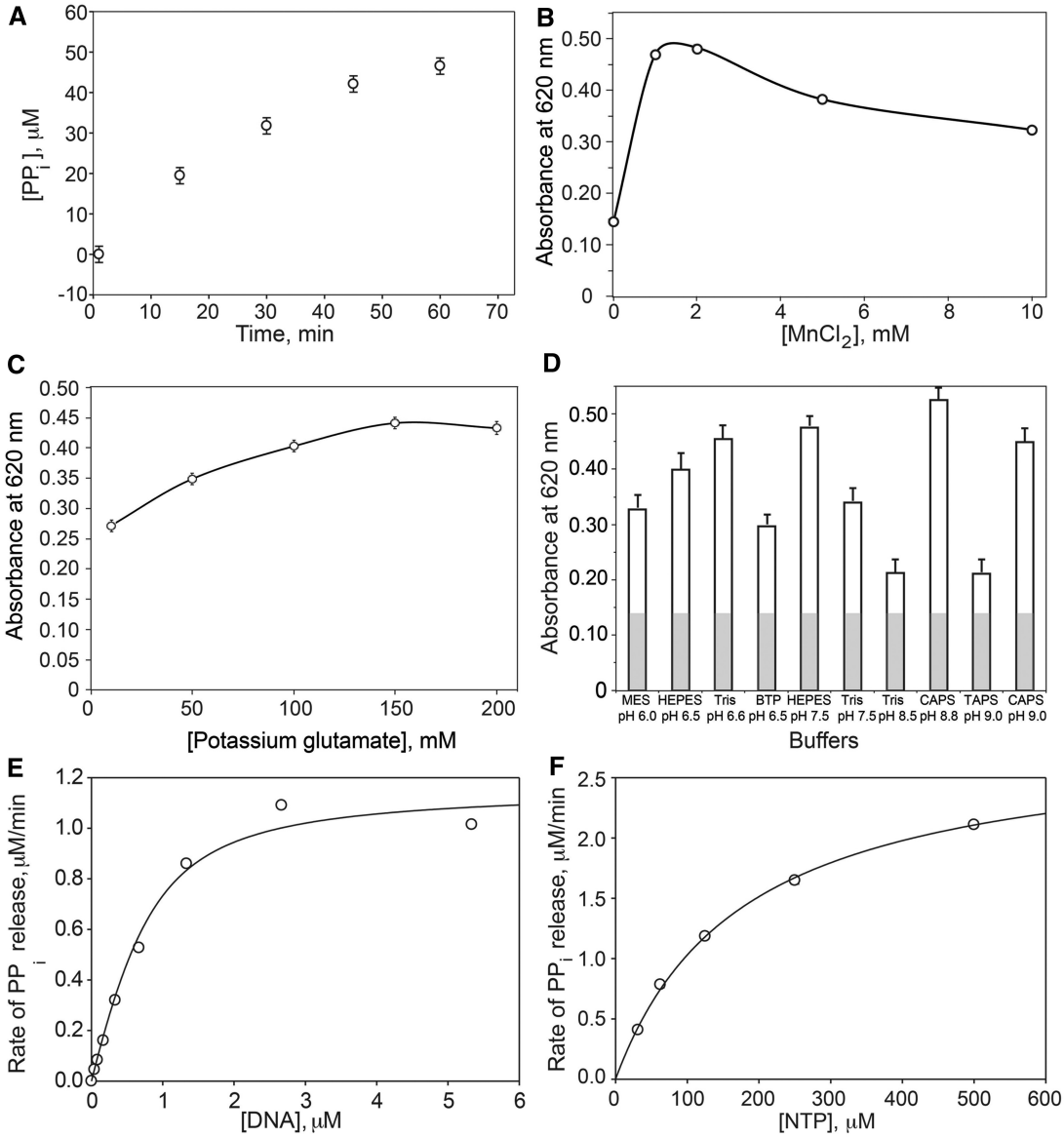

Figure 6. Optimization of conditions of the primase–pyrophosphatase assay. (**A**) A representative time course of the priming reaction, monitored by quantifying released PP_i. (**B**) Dependence of activity of *Mtb* DnaG on the concentration of $MnCl_2$. (**C**) Activity of *Mtb* DnaG as a function of the concentration of potassium glutamate. (**D**) Activity of *Mtb* DnaG in a variety of buffers (20 mM) at different pH in the range 6.0–9.0. The grey bars indicate the absorbance at time 0 in the reaction. (**E**) The steady-state rate of PP_i release during primer synthesis by *Mtb* DnaG as a function of DNA concentration. The reactions were carried out for 30 min at [*Mtb* DnaG] = 0.7 μM, [NTP] = 110 μM. (**F**) The steady-state rate of PP_i release by *Mtb* DnaG as a function of NTP concentration. The reactions were carried out for 30 min at [*Mtb* DnaG] = 0.7 μM, [DNA] = 1.25 μM.

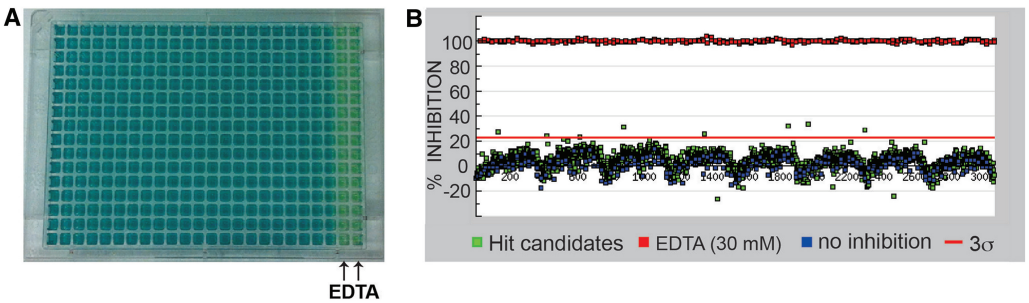

Figure 7. High-throughput coupled *Mtb* DnaG-*Mtb* PPiase assays. (**A**) A control assay used to calculate the Z' score. The last two columns of wells contain 30 mM of EDTA, used as a positive inhibition control in the HTS. (**B**) The scatterplot of the pilot assay with 2560 diverse compounds. Red squares indicate full inhibition by 30 mM of EDTA (as in panel A). Compounds that do not exhibit inhibitory properties (serving as negative controls) are shown by the blue squares, and the rest of the compounds are shown by the green squares. The red line indicates a 3σ level of inhibition, where σ is the standard deviation of the negative controls.

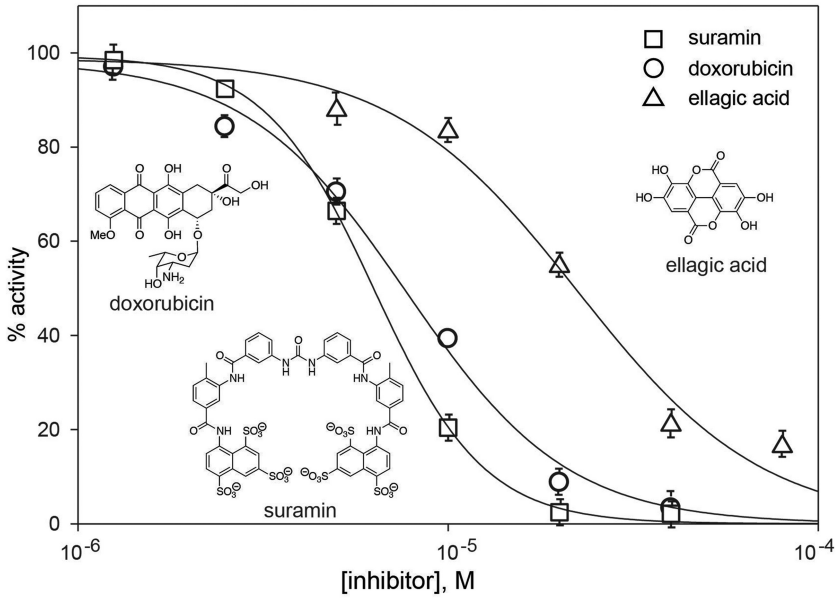

Figure 8. Dose–response assays with three hit compounds from the pilot HTS, suramin, doxorubicin and ellagic acid (the chemical structures are shown as insets). The assays were performed with 1.25 μM of DNA, 110 μM of NTP and 0.5 μM of *Mtb* DnaG.

NTP (Figure 10A and C) and the other set at a fixed concentration of NTP ([NTP] = 110 μM) with different concentrations of DNA (Figure 10B and D). The common *y*-axis intercepts in the Lineweaver–Burk plots of these data (insets in Figure 10) show that both suramin (Figure 10A and B) and doxorubicin (Figure 10B and C) are competitive inhibitors with respect to both NTP and DNA. These data effectively contain multiple dose–response curves, which, similarly to the dose–response curves presented in the previous section, indicate the presence of multiple binding sites for both suramin and doxorubicin. To obtain the equilibrium binding constant K_i and the number of sites on *Mtb* DnaG for each inhibitor, we performed a global non-linear regression analysis of these data. We used a simple assumption of multiple non-cooperative inhibitor binding sites. In addition, we used a simple approximation of an ordered sequential mechanism of priming, where an ssDNA molecule binds free *Mtb* DnaG first followed by binding of an NTP, slow primer nucleation and its rapid elongation, incorporating *m* NTP molecules per DNA-binding event. This minimal kinetic mechanism is consistent with the observed first-order kinetics of the steady-state activity of *Mtb* DnaG with respect to NTP concentration (Figure 6F) and with other data (Figure 10); the ordered binding of DNA and NTP was previously proposed for a eukaryotic primase (45). This analysis yields the values of the mechanistic parameters for *Mtb* DnaG: the catalytic rate constant $k_{cat,app} = 5.7 \pm 0.2\,min^{-1}$, the effective equilibrium constants for binding of ssDNA to *Mtb* DnaG $K_{DNA} = 24 \pm 10$ nM and for binding of an NTP to the primed DNA-*Mtb* DnaG complex $K_{NTP} = 170 \pm 10$ μM. To obtain an independent measurement of *Mtb* DnaG affinity for ssDNA, we performed a fluorimetric assay, in which increase in fluorescence polarization of a carboxyfluorescein label on ssDNA was monitored as a function of concentration of *Mtb* DnaG (Supplementary Figure S1). This assay yields equilibrium binding constant $K_d = 36 \pm 16$ nM, in good agreement with the K_{DNA} value obtained from the kinetic assays.

The aforementioned value of $k_{cat,app}$ is equal to the intrinsic k_{cat} only if the primase is completely non-processive, dissociating from DNA after incorporation of one NTP, that is, when $m = 1$. Because primases are at least somewhat processive (46,47), this value overestimates k_{cat}. In the other extreme, if *Mtb* DnaG rapidly incorporates on average 30 nt per DNA binding event, we obtain $k_{cat} = k_{cat,app}/30 = 0.19 \pm 0.01\,min^{-1}$, an underestimate of k_{cat}. The processivity of *Mtb* DnaG and the kinetics of individual NTP incorporation steps will be investigated in detail by future studies. For suramin inhibition data, an excellent fit was obtained for a minimum of $n = 4$ binding sites on *Mtb* DnaG (binding to one of which is sufficient for inhibition), with an intrinsic equilibrium binding constant for each site of $K_i = 3.2 \pm 0.5$ μM (Figure 10A and B). The analogous analysis of doxorubicin inhibition yielded best-fit values of $n = 3$ and $K_i = 2.5 \pm 0.5$ μM and also an excellent agreement with the model mechanism (Figure 10C and D). The data can also be fit well to a more complex model, where three molecules of suramin or two molecules of doxorubicin bind *Mtb* DnaG with high cooperativity (see 'Materials and Methods' section). Future studies are aimed at analysing the mechanism of inhibition of *Mtb* DnaG by these inhibitors in kinetic and structural detail.

DISCUSSION

Pioneering studies of bacterial primase DnaG 40 years ago (48,49) established this enzyme as an indispensable RNA

Figure 9. Inhibition of *Mtb* DnaG activity by suramin (S) and doxorubicin (D). The assay was performed under similar optimized reaction conditions and with the same DNA template as in the HTS and visualized and quantified as described in Figure 3.

polymerase that generates primers for chromosomal DNA synthesis *in vivo*. Since these initial studies, the primase activity has been monitored either directly, by detecting primers in gel and by high-performance liquid chromatography (50) or indirectly, by observing DNA extended from the primer by DNA polymerase or by monitoring increase in PicoGreen fluorescence on formation of an RNA–DNA hybrid (26). The use of radioactivity and gel electrophoresis or high-performance liquid chromatography for product detection impose limitations on the extent of quantitative characterization of primases and, more importantly, on our ability to exploit primases as drug targets through HTS. This study reports a novel assay that overcomes these obstacles.

Primases are intrinsically poorly processive, likely evolved so to limit the size of primers, which serve as transient substrates for initiating DNA replication, eventually getting excised by RNase H and replaced by DNA. To observe the weak primase activity *in vitro*, other stimulatory DNA replication factors, such as replicative helicase DnaB and the ssDNA-binding protein have been commonly used. With the goal of creating an orthogonal technique for detection and quantitative measurements of primase activity, we developed a non-radioactive assay, where robust activity of DnaG was achieved without its interacting partners at conditions suitable for HTS.

As *Mtb* DnaG is an important potential therapeutic target, we chose this primase and obtained it in a highly purified monomeric form; this is the first study of a mycobacterial DnaG. For coupling the primase reaction with inorganic PPiase, we chose *Mtb* PPiase. Because of its extreme specificity to PP_i, and not NTP, as a substrate, *Mtb* PPiase is exquisitely suitable for this assay. Being an essential enzyme itself, *Mtb* PPiase serves simultaneously as a second target in inhibitor discovery by HTS.

The only previous study of HTS to search for primase inhibitors was by researchers from Bristol-Myers Squibb Company, who reported a radioactive scintillation proximity DnaG activity assay with DnaB as an accessory factor for increasing activity of DnaG and as a coupled target (25). As assays using radioactivity cannot be performed in most academic screening facilities, our non-radioactive assay reported here provides a new accessible route to using DnaG as an inhibitory target in HTS. A robust performance of our coupled assay is showcased by a pilot HTS of 2556 small molecules, which yielded several confirmed hits. Three of these hits, suramin, doxorubicin and ellagic acid efficiently inhibited DnaG, the first two at a high potency. Both suramin and doxorubicin (Figure 8) contain aromatic base-like structural groups; therefore, these molecules are likely to bind the primase at a primase site (or sites) that would block DNA and/or NTP binding. Suramin was previously demonstrated to act as DNA- and NTP-competitive inhibitor of human DNA polymerase α and primase, respectively (51). Owing to its polyanionic character, suramin may interact with some of the same sites on DnaG that contact phosphate groups of the DNA backbone or incoming NTP. Quantitative analysis of inhibition by suramin and doxorubicin in this study shows that both molecules apparently compete with both DNA and NTP. We considered a simple model, where ssDNA must bind DnaG first, followed by NTP for productive RNA synthesis, similarly to the ordered binding proposed for the eukaryotic primase (45). In the framework of this model, the observed inhibitor competition with both DNA and NTP for binding the primase is interpreted as inhibitor binding to *Mtb* DnaG to block DNA binding. A more complex model where either DNA or NTP can bind free DnaG on the pathway to nucleotide transfer is also consistent with the data, and such a model is expected to yield similar K_i values. In fact, either NTP or DNA can bind to free bacterial, phage and eukaryotic primases (39,40,52–54), although NTP binding *per se* need not lead to nucleotide transfer. In any case, because this more complex model contains too many fitting parameters to be resolved by the data, it was not used in the analysis. Further studies by this and other assays are needed to clarify the order of NTP and DNA binding. Another interesting observation is that the

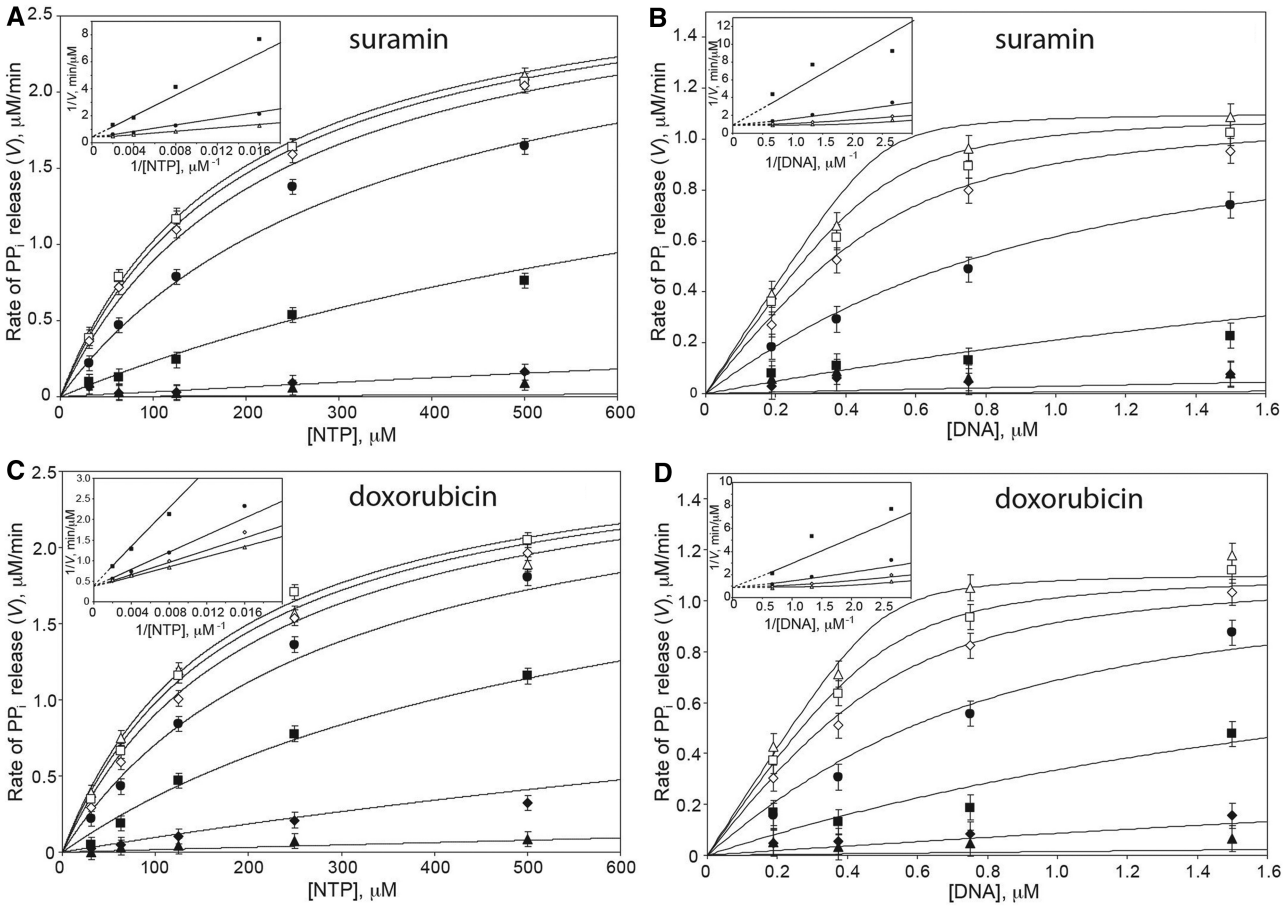

Figure 10. Measurements of the steady-state rate of PPi release on primer synthesis by *Mtb* DnaG in the presence of suramin (**A** and **B**) and doxorubicin (**C** and **D**). The assays were carried out at a fixed DNA concentration of 1.25 μM as a function of concentration of NTP (A and C) and at a fixed NTP concentration of 110 μM as a function of concentration of DNA (B and D). In all panels, the data collected without inhibitor are shown as open triangles, with 1.25 μM inhibitor as open squares, 2.5 μM inhibitor as open diamonds, 5 μM inhibitor as filled circles, 10 μM inhibitor as filled squares, 20 μM inhibitor as filled diamonds and 40 μM inhibitor as filled triangles. The insets display representative Lineweaver–Burk plots of the same data.

dependence of the steady-state activity of *Mtb* DnaG on inhibitor concentration indicates binding of multiple inhibitor molecules (four for suramin and three for doxorubicin, given the absence of cooperativity). The same intrinsic affinity is assumed for each subsequent binding event for simplicity, to keep the number of fitting parameters to a minimum. Even though this is an oversimplification, the low-μM effective K_i values and a complex stoichiometry are model-independent observations. NTP equilibrium binding constants for *Mtb* DnaG obtained from this analysis are comparable with those previously reported for other primases (55,56). Equilibrium constants for primase binding to DNA, similarly to other DNA-binding proteins, likely strongly depend on the concentration of salt and the nature of the anion (42,57,58); therefore, they are more difficult to compare. As expected for the highly optimized conditions of the assay, the K_d value for *Mtb* DnaG binding to ssDNA reported here is in the lower range of values reported for primases. For example, *E. coli* DnaG binds ssDNA with affinity of 720 nM (17), whereas *S. aureus* DnaG binds ssDNA with a six-fold greater affinity, 112 nM [as measured by the same group (50)], which is only three-fold weaker than that of *Mtb* DnaG. The K_d value that we obtained for *Mtb* DnaG is similar to the recently reported affinity (34 ± 5 nM) of *Bacillus anthracis* DnaG for an ssDNA oligomer of a similar size (19) and to the DNA-binding affinity of eukaryotic primases (45). These measurements underscore the applicability of our assay to quantitative kinetic and thermodynamic studies of primases.

In summary, the discovery of potent *Mtb* DnaG inhibitors serves as a validation of the robust assay performance in HTS. We expect that our novel assay will find applications in basic characterization of not only primases but also other inefficient nucleic acid polymerases and pave the way to a more facile HTS discovery of potent primase inhibitors. Discovery of such compounds will certainly be useful in development of clinically useful agents.

SUPPLEMENTARY DATA

Supplementary Data are available at NAR Online: Supplementary Figure 1.

ACKNOWLEDGEMENTS

The authors thank Andrew Pratt for testing inhibition of *Mtb* PPiase, Dr Luiz Pedro S. de Carvalho for a generous gift of the *Mtb* PPiase plasmid, Ahmed Mady and Shirin Shokooh for assistance with colorimetric activity assays, Tom McQuade and Dr Martha Larsen for assistance with the HTS and Dr George Garcia and Dr Garry Dotson for sharing microplate readers.

FUNDING

Seed award 2UL1TR000433-06 from the Michigan Institute for Clinical and Health Research (MICHR) and University of Michigan College of Pharmacy start-up funds (both to O.V.T.). Funding for open access charge: University of Michigan College of Pharmacy start-up funds.

Conflict of interest statement. None declared.

REFERENCES

1. van der Ende,A., Baker,T.A., Ogawa,T. and Kornberg,A. (1985) Initiation of enzymatic replication at the origin of the *Escherichia coli* chromosome: primase as the sole priming enzyme. *Proc. Natl Acad. Sci. USA*, **82**, 3954–3958.
2. Kuchta,R.D. and Stengel,G. (2010) Mechanism and evolution of DNA primases. *Biochim. Biophys. Acta*, **1804**, 1180–1189.
3. Keck,J.L., Roche,D.D., Lynch,A.S. and Berger,J.M. (2000) Structure of the RNA polymerase domain of *E. coli* primase. *Science*, **287**, 2482–2486.
4. Lipps,G., Weinzierl,A.O., von Scheven,G., Buchen,C. and Cramer,P. (2004) Structure of a bifunctional DNA primase-polymerase. *Nat. Struct. Mol. Biol.*, **11**, 157–162.
5. Augustin,M.A., Huber,R. and Kaiser,J.T. (2001) Crystal structure of a DNA-dependent RNA polymerase (DNA primase). *Nat. Struct. Biol.*, **8**, 57–61.
6. Ito,N., Nureki,O., Shirouzu,M., Yokoyama,S. and Hanaoka,F. (2003) Crystal structure of the *Pyrococcus horikoshii* DNA primase-UTP complex: implications for the mechanism of primer synthesis. *Genes Cells*, **8**, 913–923.
7. Podobnik,M., McInerney,P., O'Donnell,M. and Kuriyan,J. (2000) A TOPRIM domain in the crystal structure of the catalytic core of *Escherichia coli* primase confirms a structural link to DNA topoisomerases. *J. Mol. Biol.*, **300**, 353–362.
8. Pan,H. and Wigley,D.B. (2000) Structure of the zinc-binding domain of *Bacillus stearothermophilus* DNA primase. *Structure*, **8**, 231–239.
9. Kato,M., Ito,T., Wagner,G., Richardson,C.C. and Ellenberger,T. (2003) Modular architecture of the bacteriophage T7 primase couples RNA primer synthesis to DNA synthesis. *Mol. Cell*, **11**, 1349–1360.
10. Oakley,A.J., Loscha,K.V., Schaeffer,P.M., Liepinsh,E., Pintacuda,G., Wilce,M.C., Otting,G. and Dixon,N.E. (2005) Crystal and solution structures of the helicase-binding domain of *Escherichia coli* primase. *J. Biol. Chem.*, **280**, 11495–11504.
11. Su,X.C., Schaeffer,P.M., Loscha,K.V., Gan,P.H., Dixon,N.E. and Otting,G. (2006) Monomeric solution structure of the helicase-binding domain of *Escherichia coli* DnaG primase. *FEBS J.*, **273**, 4997–5009.
12. Bailey,S., Eliason,W.K. and Steitz,T.A. (2007) Structure of hexameric DnaB helicase and its complex with a domain of DnaG primase. *Science*, **318**, 459–463.
13. Toth,E.A., Li,Y., Sawaya,M.R., Cheng,Y. and Ellenberger,T. (2003) The crystal structure of the bifunctional primase-helicase of bacteriophage T7. *Mol. Cell*, **12**, 1113–1123.
14. Frick,D.N. and Richardson,C.C. (2001) DNA primases. *Annu. Rev. Biochem.*, **70**, 39–80.
15. Syson,K., Thirlway,J., Hounslow,A.M., Soultanas,P. and Waltho,J.P. (2005) Solution structure of the helicase-interaction domain of the primase DnaG: a model for helicase activation. *Structure*, **13**, 609–616.
16. Rowen,L. and Kornberg,A. (1978) Primase, the dnaG protein of *Escherichia coli*. An enzyme which starts DNA chains. *J. Biol. Chem.*, **253**, 758–764.
17. Swart,J.R. and Griep,M.A. (1995) Primer synthesis kinetics by *Escherichia coli* primase on single-stranded DNA templates. *Biochemistry*, **34**, 16097–16106.
18. Mitkova,A.V., Khopde,S.M. and Biswas,S.B. (2003) Mechanism and stoichiometry of interaction of DnaG primase with DnaB helicase of *Escherichia coli* in RNA primer synthesis. *J. Biol. Chem.*, **278**, 52253–52261.
19. Biswas,S.B., Wydra,E. and Biswas,E.E. (2009) Mechanisms of DNA binding and regulation of *Bacillus anthracis* DNA primase. *Biochemistry*, **48**, 7373–7382.
20. Sun,W., Schoneich,J. and Godson,G.N. (1999) A mutant *Escherichia coli* primase defective in elongation of primer RNA chains. *J. Bacteriol.*, **181**, 3761–3767.
21. Rodina,A. and Godson,G.N. (2006) Role of conserved amino acids in the catalytic activity of *Escherichia coli* primase. *J. Bacteriol.*, **188**, 3614–3621.
22. Swart,J.R. and Griep,M.A. (1993) Primase from *Escherichia coli* primes single-stranded templates in the absence of single-stranded DNA-binding protein or other auxiliary proteins. Template sequence requirements based on the bacteriophage G4 complementary strand origin and Okazaki fragment initiation sites. *J. Biol. Chem.*, **268**, 12970–12976.
23. Mendelman,L.V. and Richardson,C.C. (1991) Requirements for primer synthesis by bacteriophage T7 63-kDa gene 4 protein. Roles of template sequence and T7 56-kDa gene 4 protein. *J. Biol. Chem.*, **266**, 23240–23250.
24. Scherzinger,E., Lanka,E. and Hillenbrand,G. (1977) Role of bacteriophage T7 DNA primase in the initiation of DNA strand synthesis. *Nucleic Acids Res.*, **4**, 4151–4163.
25. Zhang,Y., Yang,F., Kao,Y.C., Kurilla,M.G., Pompliano,D.L. and Dicker,I.B. (2002) Homogenous assays for *Escherichia coli* DnaB-stimulated DnaG primase and DnaB helicase and their use in screening for chemical inhibitors. *Anal. Biochem.*, **304**, 174–179.
26. Koepsell,S.A., Hanson,S., Hinrichs,S.H. and Griep,M.A. (2005) Fluorometric assay for bacterial primases. *Anal. Biochem.*, **339**, 353–355.
27. Chen,J., Brevet,A., Fromant,M., Leveque,F., Schmitter,J.M., Blanquet,S. and Plateau,P. (1990) Pyrophosphatase is essential for growth of *Escherichia coli*. *J. Bacteriol.*, **172**, 5686–5689.
28. Bailey,K. and Webb,E.C. (1944) Purification and properties of yeast pyrophosphatase. *Biochem. J.*, **38**, 394–398.
29. Josse,J. (1966) Constitutive inorganic pyrophosphatase of *Escherichia coli*. 1. Purification and catalytic properties. *J. Biol. Chem.*, **241**, 1938–1947.
30. Pais,J.E., Bowers,K.E., Stoddard,A.K. and Fierke,C.A. (2005) A continuous fluorescent assay for protein prenyltransferases measuring diphosphate release. *Anal. Biochem.*, **345**, 302–311.
31. Lawrence,A.J., Coote,J.G., Kazi,Y.F., Lawrence,P.D., MacDonald-Fyall,J., Orr,B.M., Parton,R., Riehle,M., Sinclair,J., Young,J. *et al.* (2002) A direct pyrophosphatase-coupled assay provides new insights into the activation of the secreted adenylate cyclase from *Bordetella pertussis* by calmodulin. *J. Biol. Chem.*, **277**, 22289–22296.
32. Upson,R.H., Haugland,R.P. and Malekzadeh,M.N. (1996) A spectrophotometric method to measure enzymatic activity in reactions that generate inorganic pyrophosphate. *Anal. Biochem.*, **243**, 41–45.
33. Lloyd,A.J., Thomann,H.U., Ibba,M. and Soll,D. (1995) A broadly applicable continuous spectrophotometric assay for measuring aminoacyl-tRNA synthetase activity. *Nucleic Acids Res.*, **23**, 2886–2892.
34. Tammenkoski,M., Benini,S., Magretova,N.N., Baykov,A.A. and Lahti,R. (2005) An unusual, His-dependent family I pyrophosphatase from *Mycobacterium tuberculosis*. *J. Biol. Chem.*, **280**, 41819–41826.

35. Biswas,T. and Tsodikov,O.V. (2008) Hexameric ring structure of the N-terminal domain of *Mycobacterium tuberculosis* DnaB helicase. *FEBS J.*, **275**, 3064–3071.
36. Biswas,T., Pero,J.M., Joseph,C.G. and Tsodikov,O.V. (2009) DNA-dependent ATPase activity of bacterial XPB helicases. *Biochemistry*, **48**, 2839–2848.
37. Zhang,J.H., Chung,T.D. and Oldenburg,K.R. (1999) A simple statistical parameter for use in evaluation and validation of high throughput screening assays. *J. Biomol. Screen.*, **4**, 67–73.
38. Tsodikov,O.V., Enzlin,J.H., Scharer,O.D. and Ellenberger,T. (2005) Crystal structure and DNA binding functions of ERCC1, a subunit of the DNA structure-specific endonuclease XPF-ERCC1. *Proc. Natl Acad. Sci. USA*, **102**, 11236–11241.
39. Rymer,R.U., Solorio,F.A., Tehranchi,A.K., Chu,C., Corn,J.E., Keck,J.L., Wang,J.D. and Berger,J.M. (2012) Binding mechanism of metal-NTP substrates and stringent-response alarmones to bacterial DnaG-type primases. *Structure*, **20**, 1478–1489.
40. Lee,S.J. and Richardson,C.C. (2005) Acidic residues in the nucleotide-binding site of the bacteriophage T7 DNA primase. *J. Biol. Chem.*, **280**, 26984–26991.
41. Measures,J.C. (1975) Role of amino acids in osmoregulation of non-halophilic bacteria. *Nature*, **257**, 398–400.
42. Leirmo,S., Harrison,C., Cayley,D.S., Burgess,R.R. and Record,M.T. Jr (1987) Replacement of potassium chloride by potassium glutamate dramatically enhances protein-DNA interactions in vitro. *Biochemistry*, **26**, 2095–2101.
43. Chanley,J.D., Gindler,E.M. and Sobotka,H. (1952) The mechanism of the hydrolysis of salicyl phosphate.I[1]. *J. Am. Chem. Soc.*, **74**, 4347–4352.
44. Prinz,H. (2010) Hill coefficients, dose-response curves and allosteric mechanisms. *J. Chem. Biol.*, **3**, 37–44.
45. Sheaff,R.J. and Kuchta,R.D. (1993) Mechanism of calf thymus DNA primase: slow initiation, rapid polymerization, and intelligent termination. *Biochemistry*, **32**, 3027–3037.
46. Sun,W., Tormo,J., Steitz,T.A. and Godson,G.N. (1994) Domains of *Escherichia coli* primase: functional activity of a 47-kDa N-terminal proteolytic fragment. *Proc. Natl. Acad. Sci. USA*, **91**, 11462–11466.
47. Kuchta,R.D., Reid,B. and Chang,L.M. (1990) DNA primase. Processivity and the primase to polymerase alpha activity switch. *J. Biol. Chem.*, **265**, 16158–16165.
48. Wickner,S. and Hurwitz,J. (1974) Conversion of phiX174 viral DNA to double-stranded form by purified *Escherichia coli* proteins. *Proc. Natl Acad. Sci. USA*, **71**, 4120–4124.
49. Schekman,R., Weiner,A. and Kornberg,A. (1974) Multienzyme systems of DNA replication. *Science*, **186**, 987–993.
50. Koepsell,S.A., Larson,M.A., Frey,C.A., Hinrichs,S.H. and Griep,M.A. (2008) *Staphylococcus aureus* primase has higher initiation specificity, interacts with single-stranded DNA stronger, but is less stimulated by its helicase than *Escherichia coli* primase. *Mol. Microbiol.*, **68**, 1570–1582.
51. Ono,K., Nakane,H. and Fukushima,M. (1988) Differential inhibition of various deoxyribonucleic and ribonucleic-acid polymerases by suramin. *Eur. J. Biochem.*, **172**, 349–353.
52. Frick,D.N. and Richardson,C.C. (1999) Interaction of bacteriophage T7 gene 4 primase with its template recognition site. *J. Biol. Chem.*, **274**, 35889–35898.
53. Mustaev,A.A. and Godson,G.N. (1995) Studies of the functional topography of the catalytic center of *Escherichia coli* primase. *J. Biol. Chem.*, **270**, 15711–15718.
54. Khopde,S., Biswas,E.E. and Biswas,S.B. (2002) Affinity and sequence specificity of DNA binding and site selection for primer synthesis by *Escherichia coli* primase. *Biochemistry*, **41**, 14820–14830.
55. Urban,M., Joubert,N., Purse,B.W., Hocek,M. and Kuchta,R.D. (2010) Mechanisms by which human DNA primase chooses to polymerize a nucleoside triphosphate. *Biochemistry*, **49**, 727–735.
56. Frick,D.N., Kumar,S. and Richardson,C.C. (1999) Interaction of ribonucleoside triphosphates with the gene 4 primase of bacteriophage T7. *J. Biol. Chem.*, **274**, 35899–35907.
57. Record,M.T. Jr, Lohman,M.L. and De Haseth,P. (1976) Ion effects on ligand-nucleic acid interactions. *J. Mol. Biol.*, **107**, 145–158.
58. Ha,J.H., Capp,M.W., Hohenwalter,M.D., Baskerville,M. and Record,M.T. Jr (1992) Thermodynamic stoichiometries of participation of water, cations and anions in specific and non-specific binding of lac repressor to DNA. Possible thermodynamic origins of the "glutamate effect" on protein-DNA interactions. *J. Mol. Biol.*, **228**, 252–264.